Eur. Phys. J. D **13**, 329–336 (2001)

THE EUROPEAN PHYSICAL JOURNAL D

EDP Sciences

Study of excitation transfer Li(3D → 3P) occurring in optical collisions with rare gas atoms experimentally

G. Lindenblatt, H. Wenz, and W. Behmenburg[a]

Institut für Experimentalphysik, Heinrich-Heine Universität Düsseldorf, 40225 Düsseldorf, Germany

Received 23 February 2000 and Received in final form 5 July 2000

Abstract. By selective optical excitation of collision pairs and observation of the reemitted fluorescence information is obtained on the role of the molecular channels involved in inelelastic collisions. As an example case we have studied experimentally the Li(3D → 3P) excitation transfer in Li(3D)X systems with X = Ne, Ar by means of the optical collision process Li(2P) + X + $h\nu$ → LiX(3DΛ) → Li(3P, 3D) + X where LiX(3DΛ) collision molecules dissociate into Li(3P, 3D) atoms following laser excitation $h\nu$ of Li(2P) + X pairs. For this purpose we measured the Li 3P/3D population ratio by the fluorescence from these levels as function of the laser detuning $\Delta\nu$ from the Li(2P–3D) transition and the rare gas pressure, and determined from this the 3P/3D excitation ratio $B(\Delta\nu)$ for single collision conditions. The experiments were performed using two step cw laser excitation of gaseous mixtures Li+X at temperatures around 600 K in the detuning range $|\Delta\nu| \leq 100$ cm^{-1}. The $B(\Delta\nu)$ profiles obtained display strong blue-red wing asymmetries both for Li*Ne and Li*Ar. This reflects different dissociation probabilities from the 3DΣ or 3D(Π, Δ) states that are initially prepared by blue wing or red wing excitation, respectively. The results are qualitatively discussed in terms of new *ab initio* potentials for the two systems.

PACS. 32.70.-n Intensities and shapes of atomic spectral lines – 34.30.+h Intramolecular energy transfer; intramolecular dynamics; dynamics of van der Waals molecules

1 Introduction

In recent years an increasing number of *optical collision experiments* involving atoms at thermal energies for the study of inelastic processes like depolarisation and excitation transfer have been reported. In such experiments collision pairs (collision molecules) are selectively laser excited *during* collisions and the population distribution among the dissociated excited states is probed. Basically, by the choice of the laser frequency and due to the Franck-Condon principle the optical transition occurs at well defined distances between pairs of interatomic potentials. Thus optical collisions provide an excellent method to study the detailed dynamics of the collision following excitation and to probe sensitively the interatomic potentials involved.

So far, most optical collision spectra $M + X + h\nu \rightarrow M^* + X$ have been obtained with metal atom-rare gas systems and with the optical transitions starting from the ground states of M. By this means particularly the collision-induced fine-structure transitions and depolarisation of Na(3P) atoms has been intensively studied in cell experiments [1,2] and more recently in beams [3,4]. The very detailed information obtained from the beam experiments was analysed by means of quantum coupled channels methods [5] and yielded an almost complete picture of the detailed collision dynamics. Also recently, for the first time experimental polarisation dependent excitation spectra for excited-state $Mg^* + X$ optical collisions have been presented [6,7].

In the following we report on an optical collision experiment for the study of the 3D → 3P excitation transfer in lithium due to collisions with rare gas atoms Li(3D)+X → Li(3D, 3P) + X. For this process, total cross-sections are known from the literature [8–10], that however represent only averages of contributions from the different molecular channels 3DΛ^* → 3PΛ. To obtain channel specific information we have therefore set up an experiment, that is based on the following *optical* collision process

$$\mathrm{Li(2P)} + X + h\nu \rightarrow \mathrm{Li(3P, 3D)} + X.$$

In principle, LiX(2PΛ) collision molecules are laser excited into LiX(3DΛ^*) intermediate states, and the population ratio of the dissociated Li(3P, 3D) atoms is measured, *via* fluorescence emitted from these levels, as a function of the laser frequency ν. From the signal intensities, the branching ratio $B(\nu)$ of the atomic Li(3P, 3D) excitation along the 3DΛ → 3D and 3DΛ → 3P channels is evaluated by means of a simple rate equation system for the Li3D and 3P population. According to semi empirical potentials [11] terms 3D(Π, Δ) or 3DΣ are selectively excited depending on the laser frequency, so that from the $B(\nu)$

[a] e-mail: behmenbu@uni-duesseldorf.de

profiles information on nonadiabatic couplings specific to the different transfer channels is obtained.

The present optical collision studies at Li(2P)X differ from those at the above mentioned NaX systems in several respects. First, the optical transitions start from excited atoms other than from the groundstate. Second, the spin-orbit interaction is unimportant in the excited Li states, and besides Σ, Π also the Δ states of Li(3D)X are involved in the nonadiabatic couplings governing the 3D $\rightarrow$ 3P transfer process. Last not least, due to the large Li(3D–3P) term separation (357 cm^{-1}) the transfer probabilities are expected to be much smaller than those for the Na($3P_J$) fine structure transfer. Experimentally, this might imply severe requirements to the detection sensitivity of the Li(3P) population.

The present work was much motivated by new *ab initio* potential calculations for LiNe [12] and LiAr [13], that can be sensitively probed by the optical collision spectra for the excitation transfer in principle. Very encouraging were also concurrent quantum calculations of cross-sections for the individual 3D$\Lambda^* \rightarrow 3\Pi\Lambda$ transfer channels [17] using coupling matrix elements from *ab initio* methods [18], that facilitated at least a qualitative understanding of the experimental results. Last not least, experimental excitation spectra LiX(2P$\Lambda \rightarrow$ 3DΛ^*) recently reported [15,20] as well as measurements of integral Li(3D $\rightarrow$ 3P) transfer probabilities performed at these systems [14] permitted realistic estimations of fluorescence signal levels to be expected for given excitation and detection geometry.

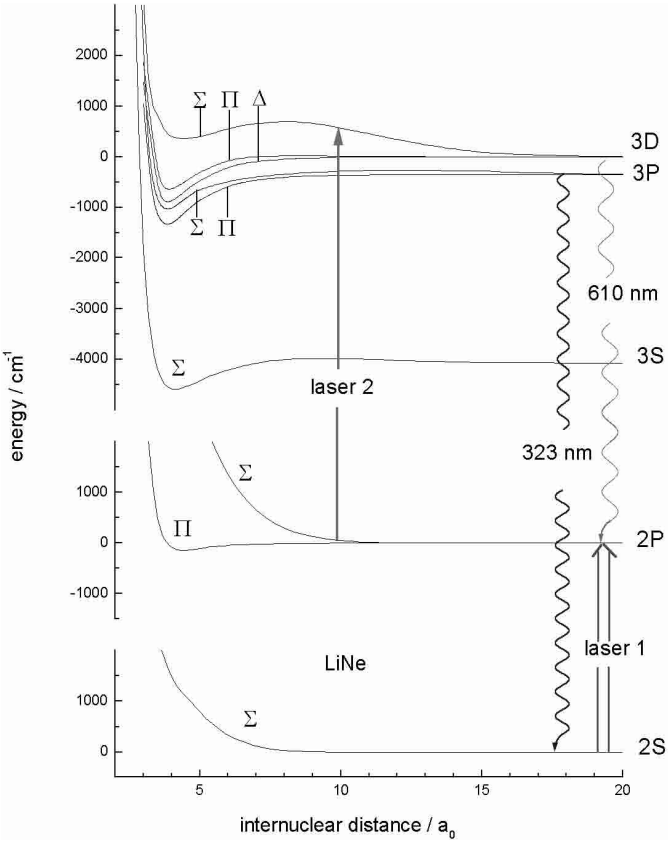

Fig. 1. Interaction potentials for the LiNe system [12] and general experimental scheme for the study of the optical collision process Li(2P) + Ne + $h\nu \rightarrow$ Li(3D, 3P) + Ne.

2 Experiment

2.1 General experimental method

The present experimental studies are based on two step cw laser excitation of gaseous mixtures of Li + X at temperatures around 600 K. The experimental scheme can be generally understood with reference to Figure 1, representing interaction potentials for the LiNe system. In this scheme laser 1 (pump laser) excites Li atoms to the 2P state, where they subsequently collide with X atoms forming collision molecules LiX(2PΛ) and a second laser (scan laser) excites these further into the higher LiX(3DΛ^*) states. According to the potentials, 3DΣ or 3D(Π, Δ) states are excited selectively at blue wing or red wing detunings respectively of the scan laser from the Li(2P–3D) transition. The subsequent dissociation LiX(3DΛ^*) $\rightarrow$ Li(3D, 3P) produces atomic Li(3D, 3P) population, which is monitored by fluorescence emission on the transitions Li(3D–2P) λ = 610 nm and Li(3P–2S) λ = 323 nm. To obtain dissociation probabilities for individual dissociation channels from the experiment, it is essential that single collision conditions are fulfilled as good as possible. Clearly, subsequent collisions of excited Li(3P, 3D) atoms before spontaneous decay would redistribute the 3P and 3D population initially present after dissociation of the LiX(3DΛ^*) collision pairs and consequently destroy channel specific information.

In such an experiment extremely small fluorescence rates, particularly at 323 nm, are to be expected for two reasons. Primarily, this results from a very small collisional 3D $\rightarrow$ 3P transfer probability 10^{-3}–10^{-4} observed [14] together with the small Einstein coefficient $A_{3P\rightarrow 2S} = 1.17 \times 10^6$ s^{-1} of the 323 nm line. Secondly this is due to extremely small off resonant excitation rates of the Li(3P, 3D) atoms resulting from two requirements: (1) rare gas number densities have to be restricted to typically 10^{16}–10^{17} cm^{-3} to keep secondary collision rates below 0.1 times the radiative decay rate from the 3D state. (2) also the Li(2P) atom density N_{2P} has to be limited, because of energy pooling collisions Li(2P) + Li(2P) $\rightarrow$ Li(3P, 3D) + Li(2S), that produce undesired extra Li(3P, 3D) excitation at rates proportional to N_{2P}^2. From these reasons a 323 nm real signal below typically 10 cps with about the same amount of energy pooling background is observed with the fluorescence detection system used (see Sect. 2.2) at scan laser detunings above 20 cm^{-1} from the 2P–3D resonance.

An additional difficulty arises due to reabsorption of the 323 nm radiation from Li2S groundstate atoms. This however can be eliminated to large extent by means of the calibration method of relative 323 nm detection sensitivity described in Section 3.

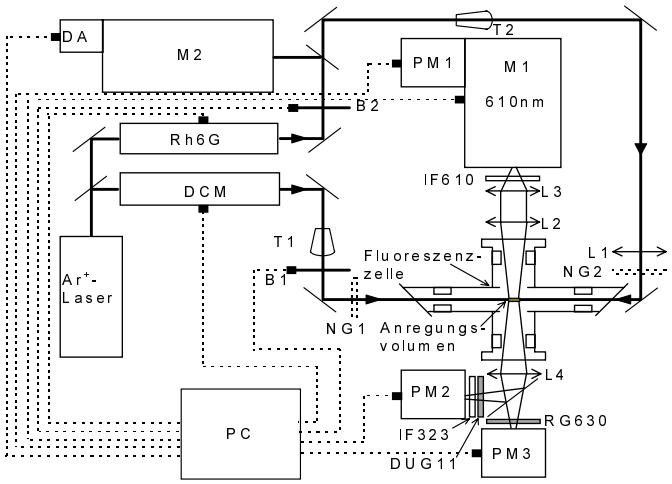

Fig. 2. Experimental setup. Rh6G: Rh6G cw dye laser, Ar^+: argon ion laser, M1, M2: monochromators, B1, B2: beam blockers, L1: BK7 glass lens, PM1: IR photomultiplier R943-02, PM3: photomultiplier R464, DUG11: metal coated filter, DCM: DCM cw dye laser, T1, T2: telescopes, DA: photo diode array, PC: personal computer, L2, L3, L4: fused silica lenses, PM2: photomultiplier 9783EMI, IF610, IF323: interference filters, RG630: glass filter, NG1, NG2: neutral glass filters.

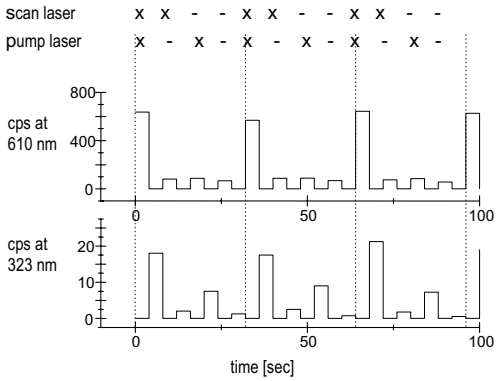

Fig. 3. Fluorescence signal rates measured alternately at $\lambda =$ 323 nm and 610 nm with different combinations of pump and scan lasers. Measurements in Li+Ne mixtures at 620 K, neon pressure 20 mbar and scan laser detuning of +20 cm^{-1}.

2.2 Experimental details

Figure 2 shows the schematic diagram of the experimental apparatus. As in earlier work [15] a stainless steel cell with cooled windows contained gaseous mixtures of saturated Li vapor with rare gas. Present measurements were performed with Ne and Ar in a pressure range 2–50 mbar at temperatures around 600 K, corresponding to densities $2 \times 10^{16}-5 \times 10^{17}$ cm^{-3}. As in reference [15] DCM and Rh6G dye lasers pumped simultaneously by a 15 W cw Ar^+ laser are used for 2-step fluorescence excitation. Both dye lasers have linear resonators CR590/599 (Coherent Radiation) and are operated multimode with bandwidths around 30 GHz and typical 50 mW at 670 nm (DCM) and 30–100 mW around 610 nm (Rh6G). Fluorescence is observed from a 10 mm overlap region of the laser beams of about 0.3 mm diameter near the center of the cell.

The main change of the present experimental arrangement as compared to that used in reference [15] concerns the fluorescence detection system required for simultaneous registration of 2 fluorescence lines emitted in widely differing spectral ranges at 323 and 610 nm with expected 323/610 intensity ratio of at most 10^{-4}.

The two fluorescence components are observed in opposite directions by means of different detection chains (Fig. 2). In forward direction the 610 nm component is separated using a 1m Czerny Turner monochromator M1 with an additional interference filter IF610 to block the leakage of 670 nm fluorescence through M1. In backward direction the 323 nm component is selected by a 320 nm interference filter IF323 and an additional cut off filter Schott DUG11 to block thermal radiation emitted from the cell walls. Photomultiplier tubes (PMT) 9783EMI and R943-02 (Hamamatsu) served as detectors for the 323 nm and 610 nm radiation, respectively. The output of the two PMT's was preamplified and processed by a single photon counting system (996 EG&G Ortec) using an electronic switch. For control of the Li(2P) pumping the 670 nm fluorescence is recorded simultaneously by means of a PMT of type R464 operated in cw current mode combined with a coloured glass filter RG630 Schott.

A major problem was the separation of fluorescence rates characteristic for the optical collision process of interest (real signals) from background signals due to instrumental stray light from the laser beams as well as fluorescence from competitive processes. For this purpose measurements at 323 nm and 610 nm were taken with different combinations of pump- and scan laser irradiation using beam blockers as illustrated in Figure 3. Signal rates were measured during 4 s alternately at the 2 wavelengths within one measurement cycle involving all possible combinations of blocked and unblocked laser beams. The number of cycles was chosen so as to obtain a preselected statistical error of the 323 nm signal rate. At an 4% error and resonant excitation (zero scan laser detuning) typical measurement time was about 10 min and increased at 10% error and 20 cm^{-1} detuning to about 1 h.

As seen from Figure 3 the largest background contribution at 323 nm is effected by the pump laser in the absence of the scan laser, *i.e.* due to energy pooling collisions of Li(2P) atoms. The Li(2P) population was therefore optimised by controlled detuning of the DCM laser within the Doppler width of the 2P–3D transition.

The real signals $S_\lambda^{\mathrm{real}}$ at 323(610) nm were obtained from the total signals S_λ^{tot} by subtraction of the background $S_\lambda^{\mathrm{b}} = S_\lambda^{\mathrm{p}} + S_\lambda^{\mathrm{s}} - S_\lambda^{\mathrm{d}}$, which inturn is composed of the signals with the beams of pump-laser S_λ^{p} or scan-laser S_λ^{s} blocked and the dark signals S_λ^{d} of the multipliers. It should be noted, that due to this procedure competitive processes leading to 3P and/or 3D population assisted by both lasers are not eliminated.

The broad band ASE background of the R6G dye laser line may excite resonantly Li(3D) states in addition to excitation by optical collisions. The contribution of such possible effect was determined by introducing a pinhole

(1 mm diameter, 2 m away from the laser outcoupling mirror) into the scan laser beam infront of the focusing lense L1a. In case of Li(2P)Ar no influence on the 323/610 nm signal ratio was found at 50 mbar Ar and -20 cm^{-1} scan laser detuning.

No effect was also observed when the laser oscillation was suppressed and the intracavity birefringent filter detuned to $+100$ cm^{-1}. The measurements with Li(2P)Ar were therefore performed without the pinhole in the beam path. With Li(2P)Ne, however, the pinhole was found to reduce the 610 and 323 nm signals significantly, *e.g.* 10% at $+20$ cm^{-1}, so it was used there for part of the measurements.

3 Calibration and control of detector sensitivities

The evaluation of the branching ratio $B(\Delta\nu)$ of Li(3P, 3D) excitation due to optical collisions from the fluorescence signals at 323 and 610 nm requires the knowledge of relative detection sensitivity $\eta_{610}^{323} := \eta_{323}/\eta_{610}$ at these wavelengths. This quantity was determined by fluorescence measurements with Li + He mixtures at 50 mbar He where the 3D and 3P populations are nearly thermalised within the excited state life times [6]. From the fluorescence signal ratio $S_{610}^{323} := S_{323}/S_{610}$ we then obtain

$$\eta_{610}^{323} = \frac{5}{3}\frac{A_{3\mathrm{D}-2\mathrm{P}}}{A_{3\mathrm{P}-2\mathrm{S}}}\exp\left[\frac{\Delta E_{3\mathrm{D}-3\mathrm{P}}}{KT}\right]S_{610}^{323} \qquad (3.1)$$

where the quantities A and ΔE are spontaneous decay rates and energy separations respectively between the indicated states. With $S_{610}^{323} = 5.6(1)\times 10^{-2}$ at 60 mbar He and $T = 585$ K, we find the value $\eta_{610}^{323} = 5.0$. This means that the 4 orders of magnitude weaker 323 nm fluorescence is detected 5 times more sensitively than the 610 nm fluorescence.

An advantage of this calibration method is the inclusion of possible trapping of the 323 nm radiation by Li(2S) atoms, although the trapping may be somewhat different for Ne and Ar as compared to He. However, the resulting integral rate coefficients for Li(3D→3P) (Tab. 2) show that reabsorption of the 323 nm fluorescence is negligible up to pressures of 20 mbar Ne or 100 mbar Ar respectively.

At given rare gas species and pressure a 10–20% long term drift of η_{610}^{323} during several weeks of cell operation was observed, that was controlled by two methods. First, before starting a spectral profile scan, the scan laser was tuned to the 3P–3D resonance and the signal ratio $\Phi := S_{323}(\mathrm{bw})/S_{323}(\mathrm{fw})$ of the 323 nm fluorescence in backward and forward direction was measured. This quantity equals the sensitivity ratio of the 323 nm detection in the two directions and a values $\Phi = 10.4(2)$ was obtained at the time of the η_{610}^{323} measurement with He. Secondly, between two scan laser detunings $\Delta\nu$ during a profile scan the signal ratio S_{610}^{323} was measured with the laser at resonance, *i.e.* $\Delta\nu = 0$.

Table 1. Einstein A coefficients and rate constants k for the collisional transfer processes Li(3D) + X → Li(3P, 3S) + X involved in the present experiments.

Li transition	$A/10^7$ s^{-1}	collisional transfer rate constant $k/10^{-13}$ cm^3 s^{-1}		
		X = Ne	X = Ar	Ref.
3D → 3P		38	5.0	[8]
3D → 3S		34	3.1	[14]
3D → 2P	7.16			
3P → 3D		26	3.4	[8]
3P → 3S	0.377		1.6	[8]
3P → 2S	0.117			

4 Evaluation of experimental data

The quantity of interest is the branching ratio $B(\Delta\nu)$ for the atomic Li(3P, 3D) excitation rates $\kappa_{3\mathrm{P}}(\Delta\nu)$ and $\kappa_{3\mathrm{D}}(\Delta\nu)$ due to optical collisions

$$B(\Delta\nu) := \kappa_{3\mathrm{P}}(\Delta\nu)/\kappa_{3\mathrm{D}}(\Delta\nu) \qquad (4.1)$$

depending on the laser detuning $\Delta\nu$ from the Li(2P–3D) resonance. The $\kappa_i(\Delta\nu)$ are inturn determined by the molecular excitation rates $\kappa_{2\mathrm{P}\Lambda\to 3\mathrm{D}\Lambda^*}(\Delta\nu)$ and dissociation probabilities $p_{3\mathrm{D}\Lambda^*\to i}(\Delta\nu)$ along the channels indicated

$$\kappa_i(\Delta\nu) = \sum_{\Lambda\Lambda^*}\kappa_{2\mathrm{P}\Lambda\to 3\mathrm{D}\Lambda^*}(\Delta\nu)p_{3\mathrm{D}\Lambda^*\to i}(\Delta\nu). \qquad (4.2)$$

The branching ratio $B(\Delta\nu)$ thus contains all information on nonadiabatic couplings during dissociation of the collision molecule following excitation.

The evaluation of $B(\Delta\nu)$ from the fluorescence signal ratio $S_{610}^{323}(\Delta\nu)$ is based on the following stationary rate equation system for population and depopulation of the Li3D and 3P levels

$$\begin{aligned}\kappa_{3\mathrm{D}} &= N_{3\mathrm{D}}\,\tau_{3\mathrm{D}}^{-1} - \gamma_{3\mathrm{P}\to 3\mathrm{D}}N_{3\mathrm{P}} + (\gamma_{3\mathrm{D}\to 3\mathrm{P}} + \gamma_{3\mathrm{D}\to 3\mathrm{S}})N_{3\mathrm{D}},\\ \kappa_{3\mathrm{P}} &= N_{3\mathrm{P}}\,\tau_{3\mathrm{P}}^{-1} - \gamma_{3\mathrm{D}\to 3\mathrm{P}}N_{3\mathrm{D}} + (\gamma_{3\mathrm{P}\to 3\mathrm{D}} + \gamma_{3\mathrm{P}\to 3\mathrm{S}})N_{3\mathrm{P}}.\end{aligned} \qquad (4.3)$$

The left hand sides of these coupled equations represent excitation rates due to optical collisions (half collisions) and the right hand sides relaxation rates due to spontaneous decay and subsequent collisions (full collisions). The quantities N, τ and γ refer respectively to the Li densities, radiative life times and the transition rates due to rare gas collisions with the states involved indicated. From equations (4.3) the stationary 3P/3D population ratio $N_{3\mathrm{P}}/N_{3\mathrm{D}} = N_{3\mathrm{D}}^{3\mathrm{P}}$ is then obtained which inturn is related to the measured fluorescence ratio S_{610}^{323}

$$S_{610}^{323} = \eta_{610}^{323}\frac{A_{3\mathrm{P}\to 2\mathrm{S}}}{A_{3\mathrm{D}\to 2\mathrm{P}}}N_{3\mathrm{D}}^{3\mathrm{P}} \qquad (4.4)$$

where the A are Einstein coefficients for the denoted transitions.

From the A values and the collisional rate constants listed in Table 1 it can be seen, that at the rare gas densities used $\gamma_{3D\to 3S} \ll \tau_{3D}^{-1}$ and $\gamma_{3P\to 3S} \ll \tau_{3D}^{-1}$. Furthermore, the experimental values of the quantity B (see Sect. 5) are small, of the order of at most 10^{-2}. From equations (4.1–4.4) and expressing rates in terms of rate constants, the measured fluorescence ratio S_{610}^{323} is then obtained as function of the rare gas density n_X with the branching ratio $B(\Delta\nu)$ as parameter to be evaluated

$$S_{610}^{323}(\Delta\nu, n_X) := \eta_{610}^{323} \frac{A_{3P\to 2S}}{\tau_{3P}^{-1} + k_{3P\to 3D} n_X} \times \left[B(\Delta\nu) + \tau_{3D} k_{3D\to 3P} n_X\right]. \quad (4.5)$$

From equation (4.5) at given detuning $\Delta\nu$ the signal ratio $S_{610}^{323}(\Delta\nu, n_X)$ in the limit $k_{3D\to 3P} n_X \ll \tau_{3P}^{-1}$ is expected to increase linearly with n_X starting from a zero density offset $S_{610}^{323}(\Delta\nu, 0)$, that contains the information about the spectral profile $B(\Delta\nu)$. The latter could therefore be determined in principle by measurements of the pressure dependence of $S_{610}^{323}(\Delta\nu, p_X)$ at different fixed $\Delta\nu$. However, at large $\Delta\nu$ and small p_X the 323 nm signal rates are below the detection limit, and at large p_X secondary collisions dominate, so that the effect of $\Delta\nu$ is small. Since however optical and secondary collisions yield independent contributions to the 3P/3D population ratio two measurements are sufficient for the determination of $B(\Delta\nu)$:

1. the spectral profile $S_{610}^{323}(\Delta\nu, p_X)$ at fixed, not too high pressure p_X. From this and equation (4.5) the difference of the B-values at nonresonant and resonant excitation is obtained as

$$B(\Delta\nu) - B(0) = \frac{1}{\eta_{610}^{323}} \frac{\tau_{3P}^{-1} + k_{3P\to 3D} p_X / k_B T}{A_{3P\to 2S}} \times \left[S_{610}^{323}(\Delta\nu, p_X) - S_{610}^{323}(0, p_X)\right]; \quad (4.6)$$

2. the pressure dependence of $S_{610}^{323}(0, p_X)$ at resonant excitation $\Delta\nu = 0$. From the slope of $S_{610}^{323}(0, p_X)$ the rate constant $k_{3D\to 3P}$ is obtained, the knowledge of which is needed for the evaluation of $B(\Delta\nu) - B(0)$ from equation (4.6). The resonant $B(0)$ value is determined from the zero pressure offset $S_{610}^{323}(0, p_X \to 0)$.

5 Results and discussion

5.1 Integral Li(3D → 3P) transfer rate coefficients and probabilities

Figures 4a and 4b represent the measured pressure dependence of the 323/610 nm signal ratio S_{610}^{323} at resonant excitation $\Delta\nu = 0$ for the two systems considered. Each point is obtained from the average result of S_{610}^{323} over a large number of runs together with error bars representing the statistical uncertainty (mainly due to photon counting statistics). In the pressure range indicated S_{610}^{323} is seen to increase very linearly with p_X starting from an offset at $p_X = 0$ in agreement with prediction for sufficiently small

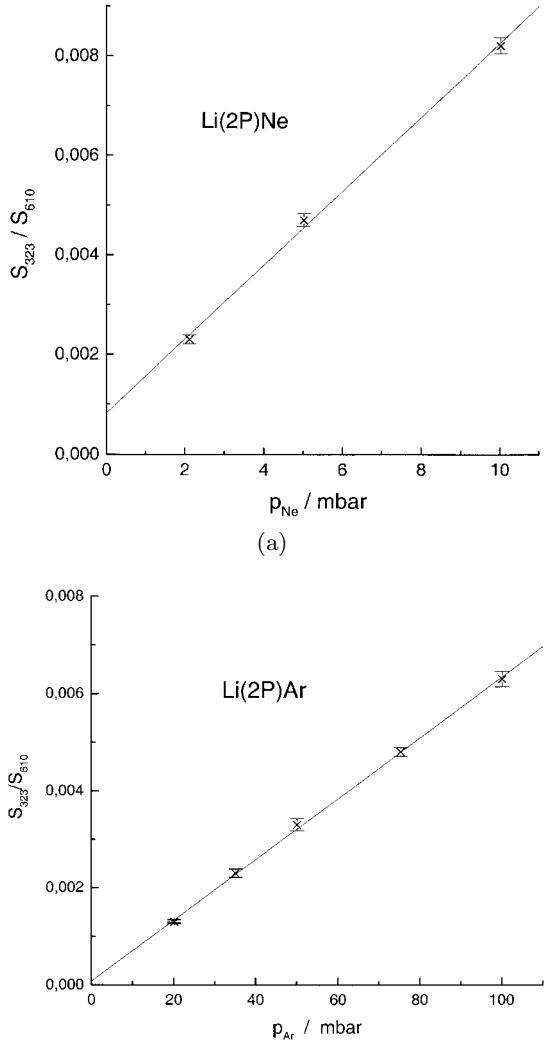

Fig. 4. 323/610 nm fluorescence signal ratio *versus* rare gas pressure at resonant excitation; (a) Li + Ne mixtures at 640 K, (b) Li + Ar mixtures at 625 K.

p_X. From the slopes of the straight line and the $p_X = 0$ intercepts together with the knowledge of the detection sensitivity ratio η_{610}^{323} the quantities $k_{3D\to 3P}$ and $B(0)$ were extracted and listed in Table 2. There also results obtained from other methods are included for comparison.

Rate coefficients

For both Li(3D)Ne and Li(3D)Ar the $k_{3D\to 3P}$ values from the present measurements at 620 K agree within error limits with the experimental values reported in reference [8] obtained at 310 K. The comparison appears to be justified at least for LiNe, because from recent quantum calculations for this system [17,18] the change of $k_{3D\to 3P}$ within the mentioned temperature interval is negligible.

Since measurements in reference [8] were performed at Li(2S) densities where trapping of the 323 nm radiation may be neglected, the good agreement indicates that

Table 2. Rate constants and branching ratios of the excitation transfer process $\mathrm{Li(3D)} + X \rightarrow \mathrm{Li(3P)} + X$.

X	$k/10^{-13}$ cm^3 s^{-1}	$B(0)/10^{-4}$	T [K]	reference
Ar	$\geq$2.6(1)		605	[14]
	4.9(6)	0.95(0.95)	620	present work
	5.0(7)		310	[8]
	$\geq$0.85		923	[9]
Ne	$\geq$26(6)		610	[14]
	46(6)	7.1(2.1)	630	present work
	38(6)		310	[8]
	17.4*			[17,18]

* $k \approx \sigma\overline{v}$, $\sigma = 1.1 \times 10^{-17}$ cm^2, $\overline{v} = 1.58 \times 10^5$ cm/s.

a possible trapping under our experimental conditions does not affect noticeably the present results.

On the other hand, our $k_{3\mathrm{D}\rightarrow 3\mathrm{P}}$ values are considerably larger than those from references [9,14] obtained at much larger Li(2S) densities where reabsorption of the 323 nm fluorescence may be considerable. The theoretical value for LiNe obtained from 2-state quantum coupled channels calculations [17,18] agrees with our experimental within a factor of 2.

The large difference of the values of $k_{3\mathrm{D}\rightarrow 3\mathrm{P}}$ for LiAr and LiNe may be qualitatively understood in terms of the interaction potentials for $3\mathrm{D}\Lambda$ and $3P\Lambda$ states of these systems. From the difference potentials given in Figure 7 it is seen that in the repulsive region $R < 4a_0$ the $3\mathrm{D}\Lambda^* - 3\mathrm{P}\Lambda$ term separations in the Li*Ar case are more than 3 times larger than with Li*Ne. Assuming Coriolis interaction to be the dominant coupling mechanism in this region may then explain the much smaller transfer rate in Li*Ar.

Probabilities

For both systems the experimental values of $B(0)$ are seen to be of the order of 10^{-3} at most, so from definitions equations (4.1, 4.2) this quantity is very nearly equal to the $3\mathrm{D} \rightarrow 3\mathrm{P}$ transfer probability $B(0) = p(3\mathrm{D} \rightarrow 3\mathrm{P})$ averaged over all molecular channels $3\mathrm{D}\Lambda^* \rightarrow 3\mathrm{P}\Lambda$. The numbers obtained may be systematically too large due to extra production of Li(3P) atoms by competitive processes in the presence of pump- *and* scan-laser. One extra contribution to 3P population may be due to energy pooling collisions Li(2S)+Li(3D) $\rightarrow$ Li(3P)+Li(2S) recently investigated experimentally [19]. According to this $N_{3\mathrm{P}}$ should scale linearly with $N_{3\mathrm{D}}$. However, an increase of the 3P/3D population ratio by only a factor 3 was observed [14] under conditions where $N_{3\mathrm{D}}$ was about 10^3 times larger than in the present experiment.

Similar to the rate coefficients also the probabilities are much larger in Li(3D)Ne than in Li(3D)Ar. However, the ratios $B(0)/k_{3\mathrm{D}\rightarrow 3\mathrm{P}}$ are found to be roughly the same for both systems within the statistical error limits. This was to be expected, since the repulsive region of the potentials, where Coriolis coupling dominates, starts at $R < 4a_0$ in both cases which means the radii of the interaction sphere are about the same.

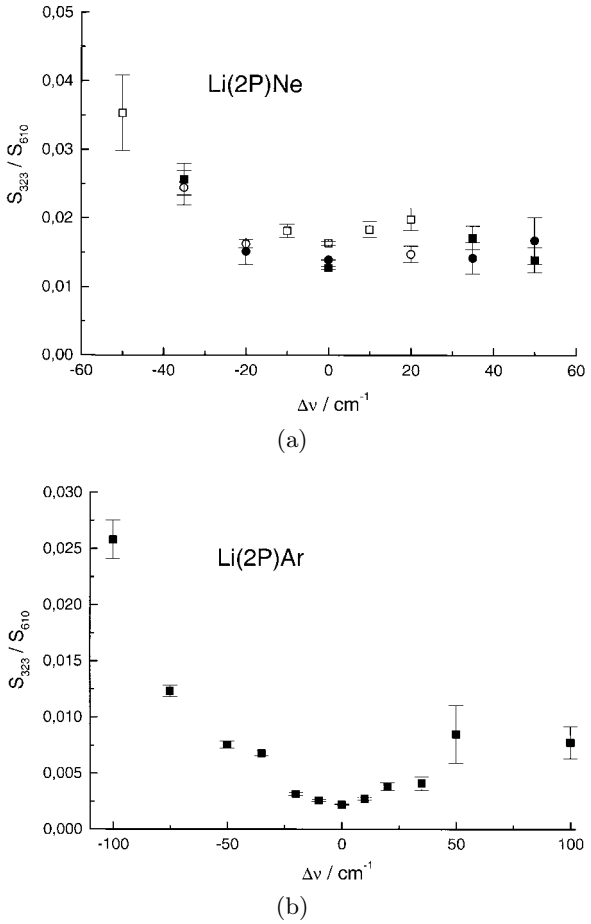

Fig. 5. 323/610 nm fluorescence ratio *versus* detuning from the Li(2P–3D) transition at 610.36 nm. (a) Li + Ne mixtures (●, ○, ■, □): independent runs of measurements at 20 mbar Ne at 625 K, (b) Li + Ar mixtures (■): at 50 mbar Ar at 620 K.

5.2 Spectral profiles

Fluorescence functions

Figures 5a and 5b represent for LiNe and LiAr the 323/610 nm fluorescence signal ratio S_{610}^{323} as function of the scan laser detuning $\Delta\nu$ from the Li 2P–3D transition. The $S_{610}^{323}(\Delta\nu)$ profile measurements at these systems were performed at different rare gas pressures chosen to optimize between large 323 nm signal rates and small contributions due to subsequent collisions. Plotted are average values of S_{610}^{323} over a great number of measurements. The errors of S_{610}^{323} indicated are due to statistical uncertainty (mainly due to photon counting statistics) of the small 323 nm real signal rates $S_{323}^{\mathrm{real}} = S_{323}^{\mathrm{tot}} - S_{323}^{\mathrm{b}}$ obtained as difference of total signal and background signal. At the off-resonant measurements typical values of S_{323}^{real} range between 2–10 cps and of $S_{323}^{\mathrm{real}}/S_{323}^{\mathrm{b}}$ between 0.3–3, decreasing with increasing detuning. In the LiNe measurements slightly differing S_{610}^{323} values at resonant excitation

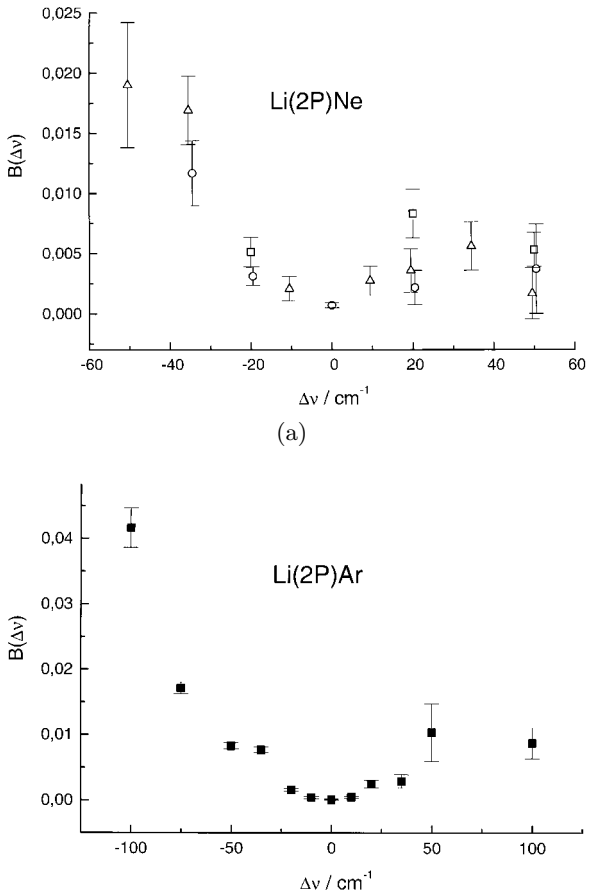

Fig. 6. Li 3P/3D excitation ratio *versus* detuning from the Li(2P–3D) transition in the optical collision process $\mathrm{Li}(2\mathrm{P}) + X + h\nu \rightarrow \mathrm{Li}(3\mathrm{P}, 3\mathrm{D}) + X$. (a) Li+Ne mixtures at 625 K, without spatial filtering: (□) $P_{\mathrm{Ne}} = 50$ mbar, (○) $P_{\mathrm{Ne}} = 20$ mbar; with spatial filtering, (△): $P_{\mathrm{Ne}} = 20$ mbar; (b) Li+Ar mixtures (■): without spatial filtering at 620 K at 50 mbar Ar.

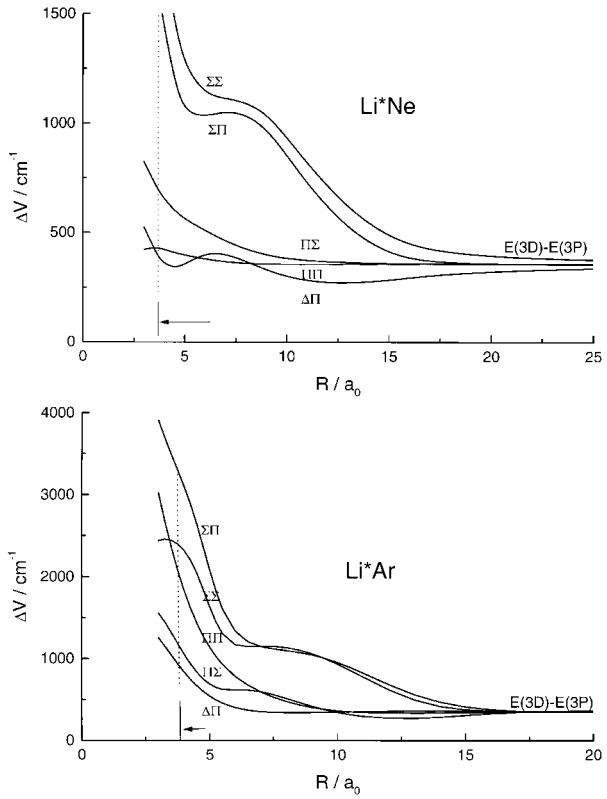

Fig. 7. Difference potentials $V(3\mathrm{D}\Lambda^*) - V(3\mathrm{P}\Lambda)$ of $\mathrm{Li}^*\mathrm{Ne}$ and $\mathrm{Li}^*\mathrm{Ar}$ systems from *ab initio* calculations in references [12,13] respectively.

$\Delta\nu = 0$ were obtained, that indicate drifts in the detection sensitivity ratio η_{610}^{323} between independent runs at different days. These drifts are taken into account in the evaluation of $B(\Delta\nu)$ according to equation (4.6).

Transfer profiles

Figures 6a and 6b display the transfer probability functions $B(\Delta\nu) = p(3\mathrm{D}\Lambda \rightarrow 3\mathrm{P}, \Delta\nu)$ obtained from the fluorescence profiles $S_{610}^{323}(\Delta\nu, p_X)$ together with the zero pressure intercept at resonant excitation $S_{610}^{323}(0, p_X \rightarrow 0)$. According to equation (4.6) the error limits of $B(\Delta\nu)$ are mainly due to the statistical uncertainties of the small signal differences $S_{610}^{323}(\Delta\nu, p_X) - S_{610}^{323}(0, p_X)$ at nonresonant and resonant excitation. In LiNe these differences were observed to be considerably smaller than in the LiAr case thus resulting in larger errors.

The effects of instrumental and physical parameters on $B(\Delta\nu)$ are demonstrated at the example case LiNe in Figure 6a. The absence of a spatial filter in the scan laser beam path tends to decrease the off-resonant $B(\Delta\nu)$ values significantly. This was to be expected, since the ASE continuum of the laser leads to additional resonant excitation that tends to reduce $S_{610}^{323}(\Delta\nu, p_X)$ and thus $B(\Delta\nu)$. Furthermore, within statistical error limits, the $B(\Delta\nu)$ values obtained at 20 mbar Ne pressure are significantly smaller than those at 50 mbar. However, accounting for a possible +1 cps systematic error of S_{323}^{b} in connection with values $S_{323}^{\mathrm{real}}/S_{323}^{\mathrm{b}} \leq 1$ at 20 mbar may reduce $B(\Delta\nu)$ up to 50% at this pressure. Thus the results at 50 mbar obtained with $S_{323}^{\mathrm{real}}/S_{323}^{\mathrm{b}} \approx 10$ should be considered as more reliable.

The $B(\Delta\nu)$ profiles of both systems are seen to increase initially with detuning from the resonance. This may be interpreted qualitatively as follows. With increasing $|\Delta\nu|$ the collision molecules are excited at decreasing Condon radius $R_{\mathrm{c}}(\Delta\nu)$ whereby smaller impact parameters $b < R_{\mathrm{c}}(\Delta\nu)$ are selected. During dissociation those molecules will therefore undergo nonadiabatic transitions $3\mathrm{D}\Lambda \rightarrow 3\mathrm{P}$ at enhanced probability.

Further in the wings the increase of the $B(\Delta\nu)$ functions is observed to be less pronounced in the blue wing than in the red wing. Also, there is indication that in the blue wings $B(\Delta\nu)$ decreases again after passing a maximum.

The experimental blue-red asymmetry of $B(\Delta\nu)$ may be qualitatively interpreted by means of the $3\mathrm{D}\Lambda^* - 2\mathrm{P}\Lambda$

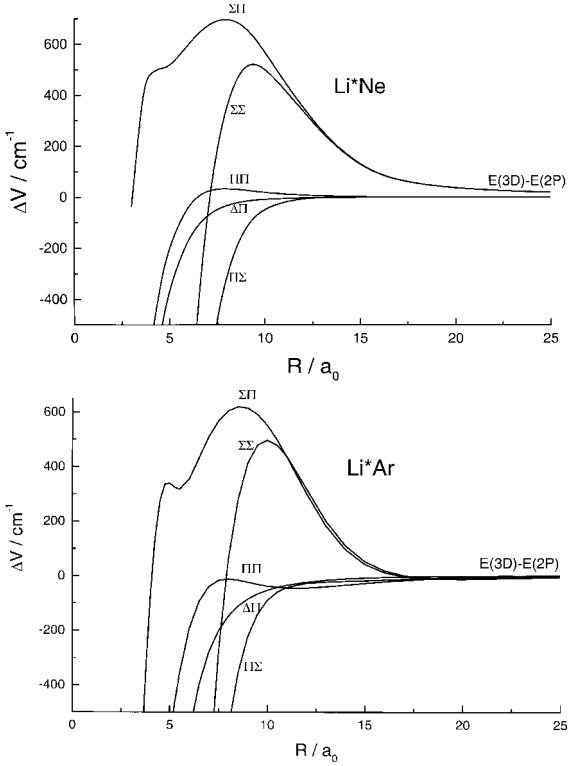

Fig. 8. Difference potentials $V(3D\Lambda^*) - V(2P\Lambda)$ of Li^*Ne and Li^*Ar from *ab initio* calculations in references [12,13] respectively.

difference potentials Figures 8a and 8b or the corresponding $\kappa_{2P\Lambda \to 3D\Lambda^*}(\Delta\nu)$ excitation functions [12] for the systems considered. It is seen that within the detuning range $|\Delta\nu| \leq 100$ cm^{-1} (beyond the impact regime) in the blue wings mainly $3D\Sigma$ states are excited and in the red wings mainly $3D(\Delta, \Pi)$ states. According to equation (4.2) the $B(\Delta\nu)$ profiles then show that the $3D \to 3P$ excitation transfer is much less efficient along the channels $3D\Sigma \to 3P\Lambda$ than along $3D(\Delta, \Pi) \to 3P\Lambda$. This finding may be qualitatively explained with much weaker Coriolis interaction to be expected in the first case: near the classical turning points $R \approx 4a_0$ of the $3D\Lambda$ potentials the energy splitting $3D\Sigma - 3P\Lambda$ is about 3–5 times larger than for $3D(\Delta, \Pi) - 3P\Lambda$.

It cannot be excluded, that the stronger increase of $B(\Delta\nu)$ in the red wing may be partly due to extra production of Li(3P) atoms by dissociation of bound $LiX(3P\Pi)$ molecules from high lying rovibronic states that are excited on the $2P\Pi \to 3P\Pi$ transitions by the scan laser. Bound state molecules $LiNe(2P\Pi)$ have been used recently for laser spectroscopy of the $2P\Pi \to 3S\Sigma$ transition in LiNe [16], and their fractional amount of about 30% at the cell temperature in the present experiments is certainly considerable. However, dipole moments for the asymptotically forbidden $2P\Pi \to 3P\Pi$ transitions into high lying rovibronic states of $3P\Pi$ are expected to be small, so that the contribution from such molecules to Li(3P) population is not believed to be dominant.

For a more quantitative understanding 2-state quantum calculations of cross-sections for all possible molecular transitions $3D\Lambda^* \to 3P\Lambda$ have been performed for the system Li(3D)Ne [17,18]. Considering both Coriolis as well as radial coupling the value 0.064 obtained for the ratio $\sigma[3D\Sigma \to 3P\Lambda]/\sigma[3D(\Delta, \Pi) \to 3P\Lambda]$ is qualitatively consistent with the different term separations mentioned above and with the *sign* of the asymmetry of the $B(\Delta\nu)$ profile observed.

A possible explanation for the blue wing maxima of $B(\Delta\nu)$ may be given by means of the following 2-step process: after excitation close to the 2P–3D resonance at large internuclear separation, the upper $3D\Lambda$ states are strongly mixed by nonadiabatic coupling during ingoing collisions. Then at smaller R nonadiabatic transitions may occur along the efficient $3D(\Delta, \Pi) \to 3P\Lambda$ channels that increase the atomic 3P population. At larger detunings $3D\Sigma$ states are increasingly selected with very small probability for $3D\Sigma \to 3P\Lambda$ transfer, that decreases the 3P population again. For testing of such a model coupled channels calculations of the optical collision rates of the $Li^*(2P)Ne$ system with inclusion of all molecular levels evolving from the excited terms in Li^* up to 3D are under way [17].

The authors are indebted to Dr. Frank Rebentrost, MPQ Garching and Prof. Martin Jungen, Institut für Physikalische Chemie, Universität Basel for making available results of their quantum calculations before publication. One of them (W.B.) would like also to thank Frank Rebentrost for valuable discussions.

References

1. M.D. Havey, F.T. Delahanty, L.L. Vahala, G.E. Copeland, Phys. Rev. A **34**, 2758 (1986).
2. W. Behmenburg, A. Ermers, F. Rebentrost, Z. Phys. D **18**, 93 (1991).
3. J. Grosser, D. Gundelfinger, A. Maetzing, W. Behmenburg, J. Phys. B **27**, L367 (1994).
4. J. Grosser, O. Hoffmann, C. Rakete, F. Rebentrost, J. Phys. Chem. A **101**, 7627 (1997).
5. F. Rebentrost, S. Klose, J. Grosser, Eur. Phys. J. D **1**, 277 (1998).
6. R.A. Lasell, S.B. Bayram, M.D. Havey, D.V. Kupriyanov, S.V. Subbotin, Phys. Rev. A **56**, 2095 (1997).
7. R.A. Lasell, D.A. Olsgaard, S.B. Bayram, M.D. Havey, D.V. Kupriyanov, Phys. Rev. A **50**, 423 (1994); *Erratum*, Phys. Rev. A **58**, 779 (1998).
8. W.J. Wang, M.D. Havey, Phys. Rev. A **29**, 3184 (1984).
9. G. Ennen, Ch. Ottinger, Chem. Phys. Lett. **88**, 487 (1982).
10. N. Yonekura, T. Nakajima, Q. Hui, M. Takami, Chem. Phys. Lett. **280**, 525 (1997).
11. J. Pascale, J. Vandeplanque, J. Chem. Phys. **60**, 2278 (1974).
12. W. Behmenburg, A. Kaiser, F. Rebentrost, M. Jungen, M. Smit, M. Luo, J. Phys. B **31**, 689 (1998).
13. W. Meyer, private communication.
14. M. Bracht, Diplomarbeit Düsseldorf, 1998.
15. A. Makonnen, A. Kaiser, W. Behmenburg, Z. Phys. D **36**, 325 (1996).
16. C.J. Lee, M.D. Havey, Phys. Rev. A **43**, 6066 (1991).
17. F. Rebentrost, private communication.
18. M. Jungen, private communication.
19. I. Labazan, S. Rudic, S. Milosevic, *ECAMP VI*, Siena, 1998.
20. A. Kaiser, Promotionsschrift Düsseldorf, 1997.